Rydberg Excitation of a Single Trapped Ion

T. Feldker,[1,*] P. Bachor,[1,2] M. Stappel,[1,2] D. Kolbe,[1,2,†] R. Gerritsma,[1] J. Walz,[1,2] and F. Schmidt-Kaler[1]
[1]*Institut für Physik, Johannes Gutenberg-Universität Mainz, Staudingerweg 7, D-55128 Mainz, Germany*
[2]*Helmholtz-Institut Mainz, Johann-Joachim-Becherweg 36, D-55128 Mainz, Germany*
(Received 19 June 2015; published 19 October 2015)

We demonstrate excitation of a single trapped cold $^{40}Ca^{+}$ ion to Rydberg levels by laser radiation in the vacuum ultraviolet at a wavelength of 122 nm. Observed resonances are identified as $3d^2D_{3/2}$ to $51F$, $52F$ and $3d^2D_{5/2}$ to $64F$. We model the line shape and our results imply a large state-dependent coupling to the trapping potential. Rydberg ions are of great interest for future applications in quantum computing and simulation, in which large dipolar interactions are combined with the superb experimental control offered by Paul traps.

DOI: 10.1103/PhysRevLett.115.173001 PACS numbers: 32.80.Ee, 37.10.Ty, 42.50.Ex

The properties of Rydberg atoms are dominated by one electron being in a state of high principal quantum number, which leads to long lifetimes and large dipole moments [1,2]. This results in giant dipolar interactions between Rydberg atoms [3] that enable the formation of ultralong-range molecules [4], quantum logic gate operations between two neutral atoms [5,6], and the control of the state of transmitted light through a Rydberg sample at the single photon level [7]. A completely new approach to this field of research is the Rydberg excitation of trapped ions [8–10], which aims to combine the long-range Rydberg-blockade mechanism, demonstrated in the case of neutral atoms [11–13], with the superb level of control over single ions achieved in Paul traps [14,15]. Rydberg ions in Coulomb crystals will allow for shaping localized vibrational modes for quantum simulation and fast parallel execution of quantum gates [16,17]. Further applications are dynamical structural phase transitions and nonequilibrium dynamics driven by Rydberg excitations [18].

Two major challenges have to be met in order to access the unique features of Rydberg ions: First, excitation energies are large compared to the case of neutral atoms, such that either a vacuum ultraviolet (VUV) laser source [9,19] or multistep excitation [20] with UV lasers is required; second, the large polarizability of Rydberg states makes them very sensitive to residual electric fields in the Paul trap, where an oscillating field with quadrupolar geometry and gradients of about 10^7–10^9 V/m^2 provides stable trapping conditions. Ions are confined near the node (field-zero) of the electric quadrupole, nevertheless residual fields at the position of the ion perturb the Rydberg state and lead to a shifted and broadened resonance.

In this Letter, we present laser excitation of a single trapped cold ion to Rydberg states. Ions are initialized in the metastable $3d^2D_{3/2}$ or $3d^2D_{5/2}$ state before they are excited to the $51F$ and $52F$ (from $D_{3/2}$), or, respectively, $64F$ (from $D_{5/2}$), state using vacuum ultraviolet radiation near 122 nm. By applying a state-dependent fluorescence measurement following the decay of the Rydberg state, population transfer out of the initial D state is detected. The polarizability of the Rydberg ion is deduced from the observed line shift and line broadening, caused by residual electric fields in the trap.

Experiments were carried out in two different linear Paul traps. Trap (A) consists of four cylindrical rods with diameter $d = 2.5$ mm at a diagonal distance of 2.2 mm, and two end caps at a distance of 10 mm [9,21]. It has a rather large trapping volume and features stable ion trapping at very low field gradients. Trap (B) is constructed from x-shaped gold-covered blades at a diagonal distance of 0.96 mm [see Ref. [22] and Fig. 1(a)]. Axial confinement is provided by applying voltages to the segments of the dc blades. The improved design of this trap allows for a more precise alignment of the electrodes. Thus, residual fields at the ion are reduced and the trap can be operated at higher vibrational frequencies as compared to trap (A). Ions are loaded from a thermal beam of neutral calcium atoms by photoionization with laser light near 423 and 375 nm. Trapped ions are illuminated by laser radiation near 397 and 866 nm for optical cooling and fluorescence detection with an electron-multiplying charge-coupled device (EMCCD) camera. Additional laser beams at 393, 854, and 729 nm allow for optical pumping, sideband spectroscopy and coherent manipulation of the $4s^2S_{1/2}$–$3d^2D_{5/2}$ transition, respectively.

Figure 1(b) shows relevant energy levels of the calcium ion. The Rydberg transition is driven by VUV single-photon excitation at 122 nm wavelength from the metastable $D_{3/2}$ and $D_{5/2}$ levels. To generate continuous-wave coherent VUV radiation we employ four-wave sum-frequency mixing in mercury vapor. Power levels in the μW range are achieved using a triple-resonant scheme with fundamental light fields at 254, 408, and 555 nm that are generated by frequency doubling and frequency quadrupling of lasers in the near infrared [9,19]. The wavelengths of these lasers are monitored by a wavelength meter (HighFinesse

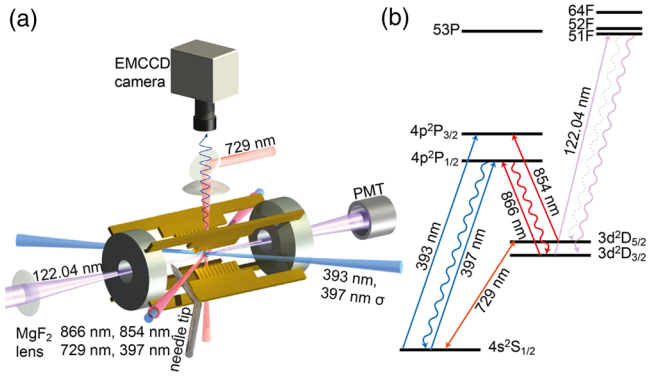

FIG. 1 (color online). (a) Sketch of the x-shaped ion trap (B) with two segmented gold-covered dc blades and two rf blades. Laser beams near 397, 866, 854, 393, and 729 nm can be switched and serve for cooling, optical pumping, and state analysis. Fluorescence light near 397 nm is collected by a lens with numerical aperture NA = 0.27 and imaged on an electron-multiplying charge-coupled device (EMCCD) camera. Holes in the end caps provide access for the VUV beam. The VUV beam intensity is monitored with a photomultiplier tube (PMT). A sharp tip can be moved into the trap for aligning the VUV beam. (b) Levels and transitions in $^{40}Ca^{+}$. Ions are cooled on the $S_{1/2}$ to $P_{1/2}$ transition near 397 nm with optical pumping on the $D_{3/2}$ to $P_{1/2}$ transition at 866 nm and initialized for the Rydberg excitation by optical pumping into the $D_{3/2}$ ($D_{5/2}$) level with light near 397 nm (393 nm).

WSU-10), which is calibrated to the $4s^2S_{1/2}$–$3d^2D_{5/2}$ transition and thus accurate to about 100 MHz at the sum frequency. The VUV radiation is focused on the ion by a pair of MgF_2 lenses and the transmitted power is monitored by a photomultiplier tube (PMT). For a precise determination of the focus we use a sharp tip that can be temporarily moved into the trap and monitor the transmission of the VUV beam. For the alignment of the beam, the MgF_2 lens closest to the trap as well as the ion trap's vacuum vessel are mounted on translation stages. Free movement between the VUV source, focusing lens, and ion trap is enabled by vacuum bellows on both sides of the lens. The MgF_2 lens additionally acts as a seal between the ion trap's ultrahigh vacuum ($<10^{-10}$ mbar) and the vacuum for transmitting the VUV radiation ($\approx 10^{-6}$ mbar).

We search Rydberg resonances at wavelengths near 122.04 nm, where the efficiency of the four-wave mixing process is strongly enhanced by the nearby 7^1S–11^1P resonance in mercury. Initial information about the expected resonances [23] could not be reproduced, and uncertainties of theory predictions [9] are too large, so that we had to search the full range of about 180 GHz between Rydberg states of consecutive principle quantum number.

Measurements have been performed with single ions and, in order to speed up data acquisition, with linear three-ion and five-ion crystals. Ions are excited to the Rydberg state in a sequence of steps. (i) Initialization by optical pumping to the $3d^2D_{3/2}$ state [lifetime 1176(11) ms [24]]. (ii) VUV excitation by a 30 ms pulse. The Rydberg state then decays and within 30 ms is either back in the initial state, the $3d^2D_{5/2}$ [lifetime 1168(9) ms [24]], or the ground state $4s^2S_{1/2}$ and the detection efficiency is therefore dominated by the branching fractions out of the initial state. (iii) Optionally, the ground state population is optically pumped into the $3d^2D_{5/2}$ state with resonant light at 393 nm. This step is necessary for detection of Rydberg P states only and was dropped after we confirmed the excitation to the Rydberg F state. (iv) Detection: Under resonant excitation with laser light at 397 and 866 nm the ion emits no fluorescence light if the Rydberg excitation in (ii) was successful. Figure 2(a) shows the observed resonance. Omitting step (iii) leads to a background free measurement since there is no population transfer from the $3d^2D_{3/2}$ state to the $3d^2D_{5/2}$ state without exciting a Rydberg resonance [the data are shown in Fig. 2(b)].

We observe Rydberg excitation to the $51F$ state at 122.041913(5) and to the $52F$ state at 122.032384 (10) nm wavelength. The linewidth of the excitation to the $51F$ varies between 60 and 400 MHz full width at half maximum (FWHM), depending on the trap control parameters. For the F resonances the branching ratio between the decay from the Rydberg state into the $D_{5/2}$ and $D_{3/2}$ state is estimated to be about 7%, using data from lower-lying Rydberg states (cf. NIST atomic spectra database). In addition to the population transfer, double ionization

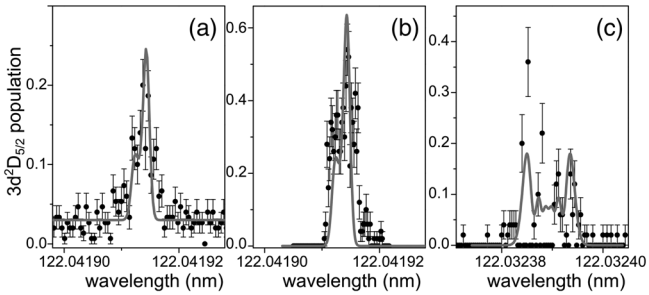

FIG. 2. (a) and (b): Rydberg excitation from the $3d^2D_{3/2}$ to the $51F$ state, at a VUV power of ≈ 0.5 μW and 30 ms pulse duration. The trap (A) is operated at motional frequencies of $\omega_{ax,rad}/(2\pi) = (90, 200)$ kHz. Different peak heights are due to variations of the VUV power and alignment for different measurement runs. (a) Ground state population is optically pumped to the $3d^2D_{5/2}$ state after the Rydberg excitation. The linewidth is $\simeq$60 MHz full width at half maximum (FWHM). (b) No optical pumping, only the direct population transfer to $3d^2D_{5/2}$ is observed. These data confirm that the Rydberg level is an F state (see text for details). (c) Excitation from the $3d^2D_{3/2}$ to the $52F$ state in trap (B), operated at motional frequencies of $\omega_{ax,rad}/(2\pi) = (270, 700)$ kHz. The line shape model includes broadening by thermal excitation, magnetic field, micromotion, and Stark effect. Measurements were performed with a single ion, 150 cycles for each data point in (a), while for (b) and (c) each data point is obtained from 50 cycles, the error bars depict the quantum projection noise.

followed by ion loss is observed on resonance in ~0.3% of the Rydberg excitations.

Higher lying Rydberg states are searched by initializing the ions in the $3d^2D_{5/2}$ state using the detection sequence described above. We do not observe population transfer exceeding the 3% background caused by the finite lifetime of the $3d^2D_{5/2}$ state. However, as in the case of the other resonances, we see significantly increased ion loss rates between wavelengths of 122.04046 and 122.04055 nm. We ascribe this ion loss to the excitation of the $64F$ state at 122.04050(5) nm. The resonance was scanned in 50 MHz steps with 50 cycles at each frequency. As the main broadening effect, polarization of the Rydberg state by residual electric fields is proportional to n^7, the resonance width of ≈2 GHz full width is in agreement with the linewidth observed for the resonances to $51F$ and $52F$.

Energy levels for Rydberg states are given by

$$E_{n,\delta} = -\frac{R_\infty}{1+\frac{m_e}{m_{\mathrm{Ca}^+}}}\frac{Z^2}{(n-\delta)^2}, \quad (1)$$

where R_∞ is the Rydberg constant, m_e is the electron mass, m_{Ca^+} is the mass of the calcium ion, Z is the charge state, and n is the principal quantum number. δ denotes the quantum defect and values from theory [25] are $\delta_F = 0.026$ and $\delta_P = 1.44$ for the F states and P states, respectively. Comparing measured excitation energies from the $3d^2D_{3/2}$ state with data from earlier experiments [23] and theory [9], the principal quantum number n can be narrowed down to be in the vicinity of 52. Applying Eq. (1) we find that the observed energy differences correspond to $n = 51$, $n = 52$, and $n = 64$ with quantum defects calculated from pairs of resonances as $\delta_{5152} = -0.08(3)$, $\delta_{5164} = 0.01(1)$, and $\delta_{5264} = 0.03(1)$. While the latter two are in agreement with theory, there is a deviation $> 3\sigma$ for δ_{5152}. This discrepancy might indicate effects beyond single channel quantum defect theory for $Ca^{2+} + e^-$ [26]. Table I shows the transition frequencies and energies determined. Measured frequencies of 411 042 130 MHz for the $4s^2S_{1/2}$–$3d^2D_{5/2}$ transition [27] and 1 819 599 MHz for the $3d^2D_{5/2}$–$3d^2D_{3/2}$ fine structure splitting [28] have been used in the data analysis. The identification of the resonances is supported by the fact that decay from the Rydberg F states is mainly into the D states as observed experimentally [see Fig. 2(b)], in contrast to Rydberg P states, which would predominantly decay into the ground state [29].

In order to model the observed resonance lines, the electric field, the motional state of the ion and the magnetic field are taken into account: Because of fabrication imperfections in the geometry of trap (A), the ion is exposed to an alternating electric field proportional to the trap drive amplitude $E_{\mathrm{geom}} = 0.8(3) \times U_{\mathrm{rf}}/\mathrm{m} \times \sin(\Omega \mathrm{t})$, where $U_{\mathrm{rf}}/\mathrm{m}$ is the applied radio frequency voltage divided by meter at the trap drive frequency $\Omega/2\pi$. This has been determined by measuring the micromotion broadening of the $4s^2S_{1/2}$–$4p^2P_{3/2}$ transition. In comparison, additional fields E_{charge} in the radial direction due to charging of electrodes by scattered VUV light are about an order of magnitude smaller when compensated optimally.

The oscillating field E_{geom} is pointing in the axial direction along the VUV laser beam, and leads to a modulation of the Rydberg energy due to the electric polarizability α, and, in addition, to a modulation of the Doppler effect due to the induced micromotion (mm). The instantaneous resonance frequency reads

$$\omega(t) = \omega_0 + k x_{\mathrm{mm}} \Omega \sin \Omega t - \frac{\alpha E_{\mathrm{geom}}^2}{2} \cos^2 \Omega t. \quad (2)$$

Here, ω_0 is the bare resonance frequency, k is the wave number of the laser along the motion of the ion, E_{geom} is the electric field amplitude, and x_{mm} is the micromotion amplitude. From this equation we can derive the temporal shape of the resonance laser field

$$E_{\mathrm{res}}(t) \propto e^{-i\omega_0 t} e^{i2\beta_\alpha \Omega t} \times \sum_n J_n(\beta_{\mathrm{mm}}) e^{in[\Omega t + (\pi/2)]} \times \sum_m (-1)^m J_m(\beta_\alpha) e^{2im\Omega t}. \quad (3)$$

In this equation we define the modulation index in the Bessel functions $J_n(\beta)$ due to the axial micromotion by $\beta_{\mathrm{mm}} = k x_{\mathrm{mm}}$ and due to the oscillating Stark shift by $\beta_\alpha = \alpha E_{\mathrm{geom}}^2/8\Omega$. The second exponent in Eq. (3) denotes a static frequency shift due to the fact that the modulated Stark shift can only reduce the transition frequency to the F states. It is apparent that the line shape comes from a complicated interplay from the sidebands at $n \times \Omega_{\mathrm{rf}}$ caused by the micromotion and the sidebands at $2n \times \Omega_{\mathrm{rf}}$ caused

TABLE I. Levels, transition vacuum wavelengths, and energies from the $S_{1/2}$ ground state.

State	Wavelength from $D_{3/2}$	Wavelength from $D_{5/2}$	ΔE cm^{-1}
$51F$	122.041913(5) nm	⋯	95 589.258(3)
$52F$	122.032384(10) nm	⋯	95 595.656(7)
$64F$	⋯	122.04050(5) nm	95 650.901(33)

by the oscillating Stark shift. Thermal ion motion at $T \approx 5$ mK, as determined from the Doppler broadening of the $4s^2S_{1/2}$–$3d^2D_{5/2}$ transition and the magnetic field of $B = 0.45$ mT, determined from the Zeeman splitting of the $4s^2S_{1/2}$–$3d^2D_{5/2}$ transition, are leading to a broadening of $\sigma \sim 10$ MHz. Thus, the line shape observed in the experiment is a convolution of Eq. (3) and a Gaussian. As the Paul trap is operated at $\Omega_{\mathrm{rf}}/2\pi$ between 3.5 and 5.2 MHz, the sidebands are not resolved in the spectrum.

With the known electric field amplitude E_{geom} we estimate α from the fit of the observed resonance line shape, the data is presented in Fig. 3(a). Calculated line shapes at various electric fields for the transitions to the $51F$ state and $51P$ state are presented in Figs. 3(b) and 3(c), the polarizabilities used in the calculation are estimated from second-order perturbation theory with neglected spin-orbit coupling. We use the quantum defects found in Ref. [25] and the method developed in Ref. [30] to obtain approximate analytical wave functions for computing matrix elements. As a check of the accuracy of this approach, we compare the calculated lifetime of the $4P$ state of 6.55 ns to the experimental value of 7 ns, which agrees reasonably well. In the second-order perturbation theory, we set $m_L = 0$, which is justified as this state experiences the largest Stark shift for the states of interest. In the calculation, we take couplings to the states $n = 40, \ldots, 60$ into account, which was found to lead to convergence.

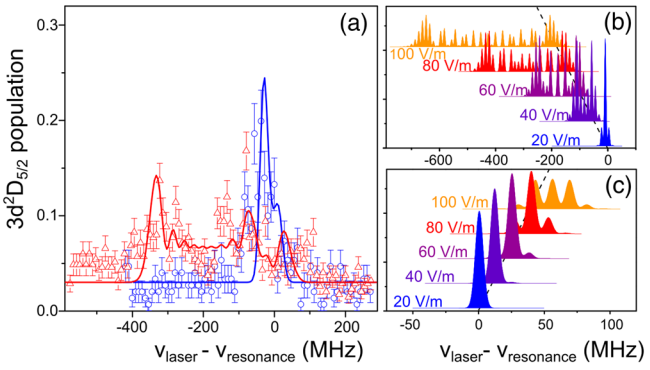

FIG. 3 (color online). (a) Experimental data [trap (A)] of the $3d^2D_{3/2}$ to $51F$ resonance with $E_{\mathrm{geom}} = 24$ (blue) and 84 V/m (red). Fitting the data with our line shape model, we determine $\alpha_{51F}/2 = 5^{+7}_{-3} \times 10^2$ MHz/(V/cm)^2 for the polarizability. Measurements were performed with one ion and 150 cycles per data point for the resonance at 24 V/m (blue) while at 84 V/m (red) a five ion crystal and 70 cycles per data point were used. The error bars depict the quantum projection noise. (b) Calculated line shapes for the $D_{3/2}$ to $51F$ transition at different residual electric fields. The axial micromotion is neglected [trap (B)] and cooling to the Doppler limit is assumed. Features of this calculation are compatible with experimental data. (c) Set of line shapes for the transition $D_{3/2}$ to $51P$ with the same parameters as in (b). Features of this calculation are incompatible with experimental data. This observation corroborates the identification of the excited Rydberg levels as F states.

The experimentally determined $\alpha/2 = 5^{+7}_{-3} \times 10^2$ MHz/(V/cm)^2 is in agreement with the polarizability of the $51F$ state, $\alpha_{51F}/2 \approx 4 \times 10^2$ MHz/(V/cm)^2 obtained from second-order perturbation theory and neglecting spin-orbit coupling. Under the assumption that the Rydberg level is the $51P$ state, the determined electric polarizability would be inconsistent with the theoretical value of $\alpha_{51P}/2 \approx -37 \times$ MHz/(V/cm)^2 from Ref. [31]. Again, this supports the identification of the Rydberg levels as F states.

In trap (B), axial micromotion is negligible, but residual electric fields E_{charge} generated by charging the surface of the trap electrodes with VUV radiation are stronger as compared to trap (A) due to a smaller distance from the ion. The resulting field is thus pointing in the radial direction and line broadening by micromotion in the direction of the VUV beam is small while the Stark effect remains the dominant line broadening effect. As this stray field E_{charge} is subjected to drifts during the run of the experiment we have not used it for polarizability measurements.

In both traps we have observed that Rydberg excitation becomes unstable after several months of experimenting. Contamination of electrode surfaces by Ca from the loading atomic beam might be an explanation for this behavior; as the work function of Ca is much smaller compared to Au, we expect a high flux of electrons from contaminated surfaces, accelerated by the rf trap. These electrons may perturb the highly susceptible Rydberg states preventing us from observing the resonance.

In the future, we plan to use a dedicated ion-loading zone well separated from the spectroscopy zone [32,33], which is shielded from the calcium beam to avoid VUV-induced photoemission of electrons close to the trapped ions. Increased VUV power and tighter focusing will allow for significantly higher excitation rates. This should enable the excitation of Rydberg P states, where the dipole matrix elements are lower by about 1 order of magnitude. Much narrower excitation resonances are expected from Rydberg P states, because the electric polarizability is lower ($\alpha_P/\alpha_F \simeq 0.1$). For a single ion in the motional ground state, and exposed to residual electric field of 65 V/m as deduced from the Rydberg resonance in trap (B), we expect a modulation index of 0.6. This results in a strong carrier and resolved sidebands at a frequency of $\pm 2 \times \Omega_{\mathrm{rf}}$ weaker by a factor of 3. In view of driving coherent dynamics, we note that with the values for VUV power of 3 μW and a waist of 10 μm already achieved, Rabi frequencies of up to $2\pi \times 150$ kHz for the transition $3d^2D_{3/2}$ to $52P$ are expected [9], which is much faster than the natural decay of 217 μs [34].

In conclusion, we have observed and identified Rydberg excitations of a single cold ion and measured the line shape of the resonance which implies a strong state-dependent coupling to the electric trapping potential.

This experimental work is a starting point for establishing a novel platform of Rydberg matter, where the unique possibilities of state-dependent electric forces as well as long-range dipole-dipole interactions are combined with the outstanding control over quantum states in trapped ion crystals.

The authors acknowledge helpful discussions with W. Li, I. Lesanovsky, P. Zoller, and M. Drewsen. We acknowledge G. Jakob and S. Wolf for support with the assembly of trap (*B*). This work was funded by the BmBF and the chist-era network (R-ION consortium) and by the European Union H2020 FET Proactive project RySQ (Grant No. 640378).

*feldker@uni-mainz.de

†Present address: Institut für Technische Physik, Deutsches Zentrum für Luft- und Raumfahrt, Pfaffenwaldring 38-40, D-70569 Stuttgart, Germany.

[1] J. M. Raimond, M. Brune, and S. Haroche, Rev. Mod. Phys. **73**, 565 (2001).
[2] M. Saffman, T. Walker, and K. Mølmer, Rev. Mod. Phys. **82**, 2313 (2010).
[3] M. D. Lukin, M. Fleischhauer, R. Cote, L. M. Duan, D. Jaksch, J. I. Cirac, and P. Zoller, Phys. Rev. Lett. **87**, 037901 (2001).
[4] V. Bendkowsky, B. Butscher, J. Nipper, J. P. Shaffer, R. Löw, and T. Pfau, Nature (London) **458**, 1005 (2009).
[5] T. Wilk, A. Gaëtan, C. Evellin, J. Wolters, Y. Miroshnychenko, P. Grangier, and A. Browaeys, Phys. Rev. Lett. **104**, 010502 (2010).
[6] L. Isenhower, E. Urban, X. L. Zhang, A. T. Gill, T. Henage, T. A. Johnson, T. G. Walker, and M. Saffman, Phys. Rev. Lett. **104**, 010503 (2010).
[7] T. Peyronel, O. Firstenberg, Q. Y. Liang, S. Hofferberth, A. V. Gorshkov, T. Pohl, M. D. Lukin, and V. Vuletic, Nature (London) **488**, 57 (2012).
[8] M. Müller, L. Liang, I. Lesanowsky, and P. Zoller, New J. Phys. **10**, 093009 (2008).
[9] F. Schmidt-Kaler, T. Feldker, D. Kolbe, J. Walz, M. Müller, P. Zoller, W. Li, and I. Lesanovsky, New J. Phys. **13**, 075014 (2011).
[10] W. Li and I. Lesanovsky, Appl. Phys. B **114**, 37 (2014).
[11] T. Amthor, C. Giese, C. S. Hofmann, and M. Weidemüller, Phys. Rev. Lett. **104**, 013001 (2010).
[12] P. Schauß, M. Cheneau, M. Endres, T. Fukuhara, S. Hild, A. Omran, T. Pohl, C. Gross, S. Kuhr, and I. Bloch, Nature (London) **491**, 87 (2012).
[13] S. Ravets, H. Labuhn, D. Barredo, L. Béguin, T. Lahaye, and A. Browaeys, Nat. Phys. **10**, 914 (2014).
[14] P. O. Schmidt, T. Rosenband, C. Langer, W. M. Itano, J. C. Bergquist, and D. J. Wineland, Science **309**, 749 (2005).
[15] R. Blatt and C. F. Roos, Nat. Phys. **8**, 277 (2012).
[16] W. Li, A. W. Glaetzle, R. Nath, and I. Lesanovsky, Phys. Rev. A **87**, 052304 (2013).
[17] R. Nath, M. Dalmonte, A. W. Glaetzle, P. Zoller, F. Schmidt-Kaler, and R. Gerritsma, New J. Phys. **17**, 065018 (2015).
[18] W. Li and I. Lesanovsky, Phys. Rev. Lett. **108**, 023003 (2012).
[19] D. Kolbe, M. Scheid, and J. Walz, Phys. Rev. Lett. **109**, 063901 (2012).
[20] M. Hennrich (private communication).
[21] T. Feldker, L. Pelzer, M. Stappel, P. Bachor, R. Steinborn, D. Kolbe, J. Walz, and F. Schmidt-Kaler, Appl. Phys. B **114**, 11 (2014).
[22] G. Jacob, K. Groot-Berning, S. Wolf, S. Ulm, L. Couturier, U. G. Poschinger, F. Schmidt-Kaler, and K. Singer, arXiv:1405.6480.
[23] C. B. Xu, X. P. Xie, R. C. Zhao, W. Sun, P. Xue, Z. P. Zhong, W. Huang, and X. Y. Xu, J. Phys. B **31**, 5355 (1998).
[24] A. Kreuter, C. Becher, G. P. T. Lancaster, A. B. Mundt, C. Russo, H. Häffner, C. Roos, W. Hänsel, F. Schmidt-Kaler, R. Blatt, and M. S. Safronova, Phys. Rev. A **71**, 032504 (2005).
[25] M. T. Djerad, J. Phys. II (France) **1**, 1 (1991).
[26] M. J. Seaton, Rep. Prog. Phys. **46**, 167 (1983), see p. 237.
[27] M. Chwalla, J. Benhelm, K. Kim, G. Kirchmair, T. Monz, M. Riebe, P. Schindler, A. S. Villar, W. Hänsel, C. F. Roos, R. Blatt, M. Abgrall, G. Santarelli, G. D. Rovera, and Ph. Laurent, Phys. Rev. Lett. **102**, 023002 (2009).
[28] R. Yamazaki, H. Sawamura, K. Toyoda, and S. Urabe, Phys. Rev. A **77**, 012508 (2008).
[29] W. Li (private communication).
[30] V. A. Kostelecký and M. M. Nieto, Phys. Rev. A **32**, 3243 (1985).
[31] A. A. Kamenski and V. D. Ovsiannikov, J. Phys. B **47**, 095002 (2014).
[32] J. Home, D. Hanneke, J. D. Jost, J. M. Amini, D. Leibfried, and D. J. Wineland, Science **325**, 1227 (2009).
[33] T. Ruster, C. Warschburger, H. Kaufmann, C. T. Schmiegelow, A. Walther, M. Hettrich, A. Pfister, V. Kaushal, F. Schmidt-Kaler, and U. G. Poschinger, Phys. Rev. A **90**, 033410 (2014).
[34] I. L. Glukhov, E. A. Nikitina, and V. D. Ovsiannikov, Opt. Spectrosc. **115**, 9 (2013).